ACS APPLIED MATERIALS & INTERFACES

Research Article

www.acsami.org

Plant Habitat-Conscious White Light Emission of Dy^{3+} in Whitlockite-like Phosphates: Reduced Photosynthesis and Inhibition of Bloom Impediment

Tomohiko Nakajima* and Tetsuo Tsuchiya

Advanced Coating Technology Research Center, National Institute of Advanced Industrial Science and Technology, Tsukuba Central 5, 1-1-1 Higashi, Tsukuba, Ibaraki 305-8565, Japan

Supporting Information

ABSTRACT: It has been pointed out that agricultural crops and other natural plants may be damaged by outdoor lighting systems. Therefore, lighting that does not affect plant growth is needed. To address this problem, we have prepared a new whitlockite-like phosphate Dy-phosphor $Ca_8MgY_{1-x-y}La_xDy_y(PO_4)_7$, which exhibits a yellow−white Dy^{3+} luminescence that has a maximum internal quantum efficiency of 65.6% under a 387 nm excitation light for $x = 0.10$ and $y = 0.05$. The x dependence of IQE showed two maxima at $x = 0.10-0.15$ and 0.80−0.85, which could be due to the partial allowance of $f-f$ forbidden transitions by local lattice distortion around the Dy^{3+} ions originating from the La incorporation at near end members of $Ca_8MgY_{1-x-y}La_xDy_y(PO_4)_7$. Concentration quenching occurred for $x > 0.05$. A white light-emitting diode (LED) was fabricated from a UV LED emitting at 385 nm and a $Ca_8MgY_{1-x-y}La_xDy_y(PO_4)_7$ phosphor (Dy-WLED) for which the CIE color coordinates and correlated color temperature were CIE(0.350,0.378) and 4919 K, respectively. Plant cultivation experiments on *Chlorella* photosynthetic growth and blooming of the short-day plant *Cosmos* were carried out using the prepared Dy-WLED and reference commercial LEDs. We found that the Dy-WLED substantially reduced the photosynthesis of *Chlorella* and inhibited bloom impediment in *Cosmos*. These effects originated especially from the reduction of red−near-IR emissions. Thus, we conclude that the Dy-WLED is a very promising candidate for plant habitat-conscious white LEDs for outdoor lights that can protect both natural plant habitats and crop yields.

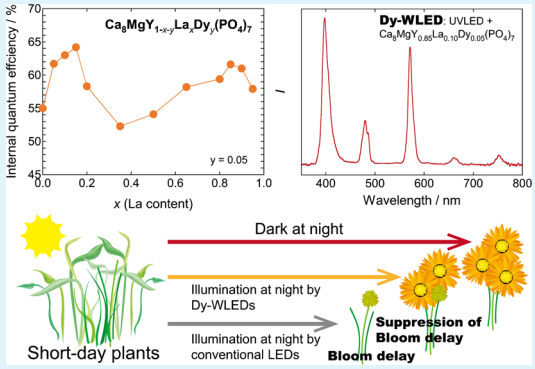

KEYWORDS: *light emitting diodes, phosphors, luminescence, Dy3+, plant growth, photosynthesis, bloom impediment*

1. INTRODUCTION

Throughout human history, lighting has been developed to improve quality of life. Ever since the invention of incandescent lamps by Edison in 1879, electric lights have been used for many applications including residential lights, outdoor lamps, displays, and biocultivation in plant factories. With the expansion of these applications, various types of lighting systems, such as mercury and fluorescent lamps, have been developed. The recent progress of light-emitting diodes (LEDs) is a significant breakthrough because of their very long lifetime and high luminous efficacy compared with conventional lighting systems.[1−3] White LEDs (WLEDs) are usually formed by blue LEDs and either yellow phosphors (YB)[2,4] or red/green phosphors (RGB).[5,6] Therefore, much research into WLEDs has been devoted to making phosphors that emit light that is brighter and more comfortable for human eyes.[3,7−10]

However, there are negative effects on the natural environment from outdoor lighting systems. Natural plant habitats, particularly at dark sites such as caves and forests, can be destroyed because the increase in illumination intensity allows different species to thrive.[11] This is a significant problem for the protection of native species and the preservation of natural heritage that needs to be addressed. Moreover, light during the nighttime prevents the flowers of short-day plants from blooming and accelerates bolting in long-day plants. These damage natural plant habitats and decrease crop yields.[12,13]

Therefore, artificial lighting systems must consider the protection of plant habitats, and lighting that does not affect plant growth must be developed.[14] With this aim, we have fabricated a plant habitat-conscious WLED (PHC-WLED) using Dy^{3+} luminescence. In this paper, we describe the structural and optical properties of a new bright Dy-phosphor $Ca_8MgY_{1-x-y}La_xDy_y(PO_4)_7$ (CMYLP:Dy) that had good internal quantum efficiency (IQE) of 65.6% under 387 nm excitation. This IQE is among the highest compared with the previously reported values for Dy-phosphors (Table 1). We also report plant cultivation tests using a WLED consisting of the CMYLP:Dy phosphor and an excitation UV LED and show

Received: July 10, 2015
Accepted: September 10, 2015
Published: September 10, 2015

DOI: 10.1021/acsami.5b06208
ACS Appl. Mater. Interfaces 2015, 7, 21398−21407

Table 1. IQE and Excitation Wavelength (λ_{exc}) of Dy-Phosphors

phosphors	IQE	λ_{exc}	ref
$Ca_8MgY_{0.85}La_{0.10}Dy_{0.05}(PO_4)_7$	65.7%	387 nm	this work
$LiLa_{0.90}Dy_{0.10}P_4O_{12}$	76%		16
$Ca_{2.95}Dy_{0.05}Si_2O_7$	15.2%	365 nm	17
$GdNbO_4$:Dy	21.7%	270 nm	18
Y_2WO_6:Dy	17%	302 nm	19
$AgY_{0.98}Dy_{0.02}(WO_4)_2$	56%	270 nm	20
$Li_3Ba_2Y_{2.90}Dy_{0.10}(MoO_4)_8$	20%	388 nm	21
$K_2Y_{0.97}Dy_{0.03}(WO_4)$ (PO_4)	21.0%	389 nm	15

its effect on reducing photosynthesis.[15] Moreover, we have discovered that the Dy^{3+} luminescence also inhibits blooming impediment in short-day plants.

2. EXPERIMENTAL SECTION

Polycrystalline CMYLP:Dy phosphors were synthesized by a solid-state reaction. A mixture of reagent powders, namely, $CaCO_3$, MgO, Y_2O_3, La_2O_3, $(NH_4)_2HPO_4$, and Dy_2O_3 in an appropriate molar ratio, was preheated at 700 °C for 2 h in air. After an intermediate grinding, the precursors were heated at 1300 °C for 6 h in air. The samples were cooled down to room temperature with a rate of 200 °C/h. The La and Dy substitutions were carried out at the Y sites. The products were confirmed to be a single phase of $Ca_8MgY_{1-x-y}La_xDy_y(PO_4)_7$ by X-ray diffraction (XRD; RINT-2000, Rigaku). The crystal structure was refined by Rietveld analysis using RIETAN-FP.[22] The schematic crystal structure of CMYLP:Dy was drawn in VESTA.[23] The crystal morphology of the sample was examined using field-emission scanning electron microscopy (FESEM; SU9000, Hitachi). The photoluminescence spectrum, the IQE, IQE excitation spectrum, and the luminescence color properties of the samples were evaluated with a C9920−02 spectrometer (Hamamatsu Photonics) equipped with a xenon lamp, a monochromator, a back-illuminated multichannel charge-coupled device photodetector, and an integrating sphere. The IQE (%) was calculated as IQE = $N_{em}/N_{abs} \times 100$, where N_{em} and N_{abs} are the numbers of emitted and absorbed photons, respectively.

A WLED containing the Dy-phosphor (Dy-WLED) was prepared by embedding the CMYLP:Dy powder into silicone resin coated onto a power UV LED (NS385L-6SMG, Nitride Semiconductors). The excess UV light from the Dy-WLED was removed with a UV cut filter (λ < 400 nm) to eliminate an extra influence for plant growth. Three other commercial WLEDs were used for comparison. The color properties, spectral irradiance, and illuminance for all LEDs were studied using a multichannel spectrometer USB2000+ (Ocean Optics) with a light-collecting optical fiber.

An experiment on *Chlorella* cultivation with the Dy-WLED and three reference LEDs was performed. The *Chlorella* cells were dispersed in a 0.1% HYPONeX (HYPONeX Japan Co., Ltd.) aqueous solution, and then it was filtered to remove aggregated colonies by using a coarse textured paper filter. The homogeneously dispersed *Chlorella* solution was optically transparent. *Chlorella* solution (3 mL) in a transparent cell was placed in a container covered with aluminum foil inside to guarantee the light spectra originated from only the LED, and then it was illuminated with an LED under equivalent illuminance (200 lm m^{-2}) conditions at 27 °C (Figure S1). The weight of the *Chlorella* was measured after drying the solution overnight at 60 °C.

An experiment on flower blooming with the Dy-WLED and three reference LEDs was carried out on *Cosmos sulphureus Cav.* (*Cosmos*) as a model of short-day plants. The *Cosmos* were hydroponically cultivated in containers covered with aluminum foil inside as in the *Chlorella* breeding and illuminated by a fluorescent lamp that emitted simulated sunlight in the visible light range at 8 k lm m^{-2} for 8 h from 9:00 to 17:00 every day. For 16 h from 17:00 to 9:00, the four containers were illuminated by the Dy-LED or reference LEDs at 50 lm m^{-2}, and one container was kept dark (<0.5 lm m^{-2}) as a control (Figure S1). The culture solution was 0.1% HYPONeX water, and it was renewed once each week. The flower numbers were counted for three plants illuminated by each LED and the control (kept in the dark).

3. RESULTS AND DISCUSSION

3.1. Structural and Luminescence Properties of CMYLP:Dy. Figure 1, panel a shows the XRD 2θ scan and

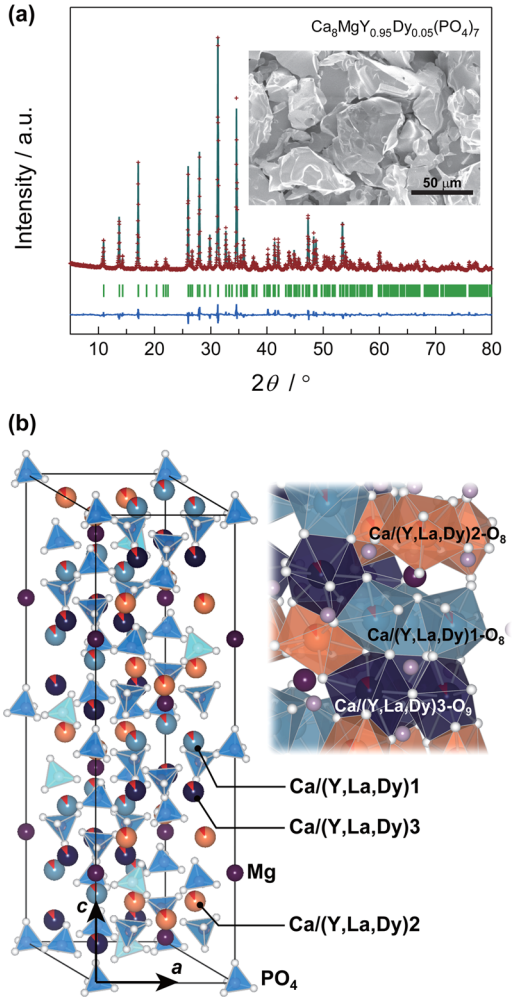

Figure 1. (a) XRD 2θ/ω scan of $Ca_8MgY_{0.95}Dy_{0.05}(PO_4)_7$. Calculated and observed diffraction profiles are shown at the top by the solid line and crosses, respectively. Vertical marks in the middle show the positions of the calculated Bragg reflections. The lower trace is a plot of the difference between the calculated and observed intensities. The inset shows the FESEM image of polycrystalline morphology of $Ca_8MgY_{0.95}Dy_{0.05}(PO_4)_7$. (b) The schematic crystal structure of $Ca_8MgY_{1-x-y}La_xDy_y(PO_4)_7$.

FESEM image of the CMYLP:Dy (x = 0.00 and y = 0.05) powder. All the XRD peaks were indexed to a hexagonal unit cell of whitlockite-like structure. The polycrystalline grains were relatively large with the size of about 50 μm, and there was not distinctly different morphology from the main phase. Therefore, we assumed that the obtained sample was the single phase of whitlockite-like phosphates in this study, though trace amorphous phases are possible within our target phase, as indicated in previous work by Adcock et al.[24] Rietveld refinement was performed for the obtained XRD patterns, and they were successfully fitted as an isostructure to $Ca_9Eu(PO_4)_7$[25] crystallized with the space group $R3c$ (No.

DOI: 10.1021/acsami.5b06208
ACS Appl. Mater. Interfaces 2015, 7, 21398−21407

Table 2. Structural Parameters for CMYLP:Dy (x = 0.00 and y = 0.05)[a] Refined by Rietveld Analysis of Powder XRD at Room Temperature

space group	*R3c* (161)		2θ range (°)		5.0−80.0
symmetry	trigonal (hexagonal setting)		number of reflns		2501
a(Å)	10.3649(1)		R_{wp} (%)		9.673
c (Å)	37.0770(4)		R_p (%)		7.502
V (Å^3)	3449.58(6)		R_e (%)		6.016
atom	Wyck.	g	x	y	z	B_{iso} (Å^2)
Ca1	18b	0.850(7)	0.7245(5)	0.8695(9)	0.1640(3)	0.383
Ca2	18b	0.892(7)	0.6232(6)	0.803(1)	0.9624(3)	0.383
Ca3	18b	0.925	0.7211(5)	0.8708(8)	0.0568(3)	0.383
YLaDy1	18b	0.150	0.7245	0.8695	0.1640	0.383
YLaDy2	18b	0.108	0.6232	0.803	0.9624	0.383
YLaDy3	18b	0.075	0.7211	0.8708	0.0568	0.383
Mg	6a	1	0	0	0.7327(6)	0.382
P1	6a	1	0	0	0	0.194
P2	18b	1	0.6818(6)	0.828(1)	0.8667(4)	0.194
P3	18b	1	0.6522(9)	0.801(1)	0.7641(3)	0.194
O1	18b	1	0.733(1)	0.827(1)	0.9042(5)	0.462
O2	18b	1	0.733(2)	0.732(2)	0.8442(6)	0.462
O3	18b	1	0.754(2)	0.982(2)	0.8539(6)	0.462
O4	18b	1	0.516(1)	0.763(3)	0.8649(7)	0.462
O5	18b	1	0.827(1)	0.899(2)	0.7761(6)	0.462
O6	18b	1	0.576(2)	0.880(2)	0.7828(6)	0.462
O7	18b	1	0.605(2)	0.655(2)	0.7789(6)	0.462
O8	18b	1	0.633(1)	0.809(2)	0.7242(5)	0.462
O9	18b	1	0.127(1)	0.984(1)	0.9868(6)	0.462
O10	6a	1	0	0	0.0419(6)	0.462

[a]Labels x and y represent the mixture of Y, La, and Dy ($Y_{1-x-y}La_xDy_y$). The fractions of these ions were fixed to x = 0.00 and y = 0.05 in this calculation. Atomic positions of YLaDy1 − YLaDy3 were restricted to the Ca1−Ca3 sites, and the fraction ratio of Ca:YLaDy was kept as 8:1.

161) (Figure 1a). The fitting reliable factors were R_{wp} = 9.673%, R_p = 7.502%, and R_e = 6.016%. This structure is originally derived from the merrillite β-$Ca_3(PO_4)_2$ that has six Ca sites (M1−M6).[26] Each site has different coordination environments: the M1 and M2 sites have eight oxygen coordinates, the M3 and M5 sites have nine and six oxygen coordinates, respectively, and the M4 and M6 sites are usually vacant.[26−28] In CMYLP:Dy, the M1, M2, M3, and M5 sites can be occupied by Ca^{2+} (r (ionic radius) = 1.120 Å, coordination number (CN): 8), Mg^{2+} (r = 0.890 Å, CN: 8), Y^{3+} (r = 1.019 Å, CN: 8), La^{3+} (r = 1.160 Å, CN: 8), and Dy^{3+} (r = 1.027 Å, CN: 8)[29] ions. Since the M5 site, which has six oxygen coordinates, would be occupied by smallest ion Mg^{2+}, the other ions (Ca^{2+}, Y^{3+}, La^{3+}, and Dy^{3+}) were assigned to the M1−M3 sites in the structural refinements (Figure 1b, Figure S2 and Table S1). Table 2 shows the refined structural parameters of CMYLP:Dy (x = 0.00 and y = 0.05).

Figure 2 shows the structural parameters a, c, V and occupancy of rare earth (RE: Y, La and Dy) ions at the M1−M3 sites. The La ion incorporation (variation of x) to the Y site in CMYLP:Dy (y = 0.05) created all proportional solid solutions; however, the x dependence of lattice parameters did not follow Vegard's law at two points near each end (x = 0.10 or 0.80). At x = 0.10 and 0.80, the lattice parameters a and c were very slightly (ca. 0.1%) shrunk and elongated, respectively, from the lines predicted from Vegard's law. The site occupancy of RE ions varied as a function of x: the occupancies of M1 and M2 gradually decreased, and that of M3 increased with increasing x, without any anomaly. The increasing fraction of large La ions at the M3 site was caused by the large size capacity of this site due to the nine oxygen coordinates. This tendency, in which large ions favorably occupy the M3 sites, is consistent with a previous report.[27] The M−O bond lengths as a function of x were evaluated and are shown in Figure 3. The x dependences of M1(M2)−O and M3−O lengths were convex upward and downward, respectively. The averaged M−O bond length, taking site occupancies of RE ions into account, showed a gradual increase as a function of x without an obvious anomaly at x = 0.10 or 0.80.

Figure 4, panel a shows a photoluminescence spectrum of CMYLP:Dy (x = 0.10 and y = 0.05) under excitation at 385 nm. The CMYLP:Dy exhibited a yellowish white luminescence, and sharp emission peaks were observed at 480, 571, 661, and 751 nm that can be assigned, respectively, to the $^4F_{9/2} \rightarrow {}^6H_{15/2}$, $^4F_{9/2} \rightarrow {}^6H_{13/2}$, $^4F_{9/2} \rightarrow {}^6H_{11/2}$, and $^4F_{9/2} \rightarrow {}^6H_{9/2}$ transitions in Dy^{3+} ions. The luminescence CIE color coordinates (CIE(x, y)) and correlated color temperature (CCT) excited at 385 nm were estimated to be CIE(0.386, 0.439) and 4236 K, respectively. Among the luminescence transitions in CMYLP:Dy, the $^4F_{9/2} \rightarrow {}^6H_{13/2}$ transition was dominant. This would be caused by the low symmetry of the 18b site in the *R3c* space group without inversion center (C_1 point symmetry), where the Dy^{3+} ion was located. It has been reported that the $^4F_{9/2} \rightarrow {}^6H_{13/2}$ transition of Dy^{3+} is very sensitive to the crystal-field environment: this transition can be enhanced when the Dy^{3+} occupies sites with low symmetry.[16,30,31] The IQE excitation spectrum for CMYLP:Dy (x = 0.10 and y = 0.05) is shown in Figure 4, panel b. In this spectrum, four excitation bands were observed at 325, 351, 365, and 387 nm that can be assigned, respectively, to the $^6H_{15/2} \rightarrow {}^6P_{3/2}$, $^6H_{15/2} \rightarrow {}^6P_{7/2}$, $^6H_{15/2} \rightarrow {}^4D_{5/2}$, and $^6H_{15/2} \rightarrow {}^4M_{21/2}$ transitions in Dy^{3+} ions. The maximum IQE was 65.6% at 387

DOI: 10.1021/acsami.5b06208
ACS Appl. Mater. Interfaces 2015, 7, 21398−21407

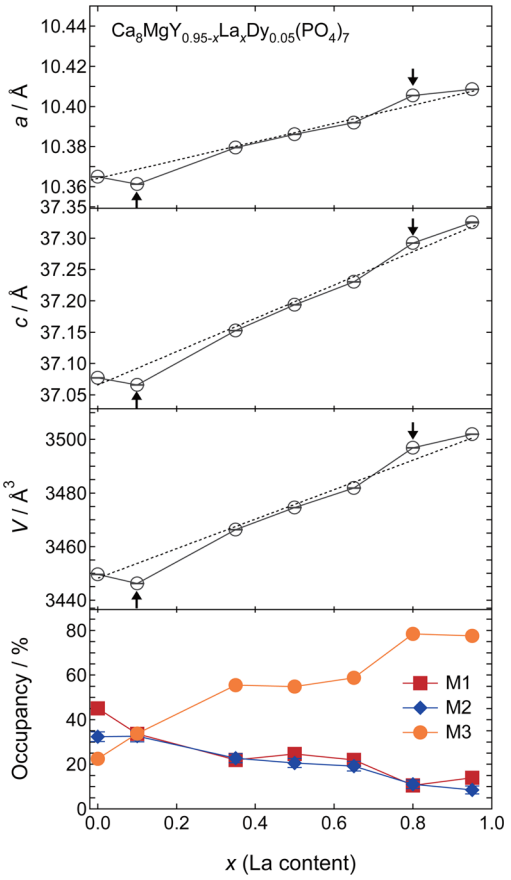

Figure 2. Refined structural parameters and site occupation at M1–M3 sites for RE ions in CMYLP:Dy.

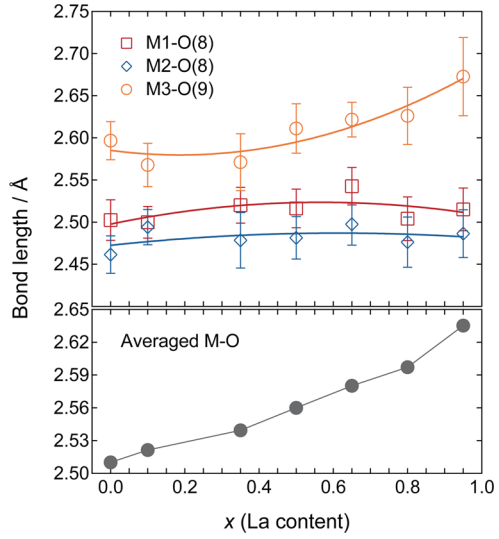

Figure 3. M1–O, M2–O, M3–O, and averaged M–O bond lengths in CMYLP:Dy.

nm. Interestingly, two IQE and 571 nm luminescence intensity ($I_{571\ nm}$) maxima were confirmed at x = 0.15 and 0.85 for the IQE and at x = 0.10 and 0.80 for the $I_{571\ nm}$ (Figure 4c). The IQE and $I_{571\ nm}$ around x = 0.10–0.15 were, respectively, 18% and 51% higher than those of the nearby end member at x = 0.00. From the structural refinements, no specific variation was confirmed in the atomic coordinates of averaged crystal structures at around x = 0.10–0.15 and 0.80–0.85, while the lattice parameters had anomalies at x = 0.10 and 0.80 (Figures 2 and 3). The f–f transition of Dy^{3+} should be partially allowed by lowering local symmetry.[32] The occupation sites of Dy^{3+} ions (M1–M3) had lowest point symmetry C_1 without inversion center regardless of the Y^{3+}/La^{3+} ratio. It has been known that the randomly distributed two ions that have a large difference of ionic radii at same crystallographic site can vary the local electrostatic potential by local lattice distortion around those sites, which cannot be discussed from an assumption of the averaged crystal structure.[33,34] Therefore, we hypothesized that a partial allowance of forbidden f–f transition due to the local lattice distortion produced by minor incorporation of ions to the end members, which had a relatively large difference of ionic radii between the La^{3+} and Y^{3+} (Dy^{3+}), could be the main cause of luminescence enhancement.

The IQE under excitation at 385 nm increased with x from 0.01 to 0.05 and then decreased (Figure 4d). Thus, we identified CMYLP:Dy (x = 0.10 and y = 0.05) as the optimum composition for the brightest luminescence. From the concentration quenching behavior, the critical distance (R_C), which is the distance between the activator and the quenching site for the most efficient energy transfer, can be evaluated by using the Blasse equation:[35]

$$R_C = 2\left(\frac{3V}{4\pi X_C N}\right)^{1/3}$$

where V is the volume of the unit cell, X_C is the critical concentration of Dy^{3+}, and N is the number of substituent sites for the dopant in the unit cell. For the CMYLP:Dy host, V = 3446.15 Å^3, X_C = 0.05 at the maximum IQE, and N = 54; consequently, R_C is calculated to be 13.46 Å. The exchange interaction generally restricts the critical distance to around 5 Å when it is dominated by an energy transfer.[36,37] The value of R_C was relatively large in this case; therefore, the multipolar interaction was the dominant mechanism for the concentration quenching in the CMYLP:Dy phosphors. In the plot of $\log(I/y)$ versus $\log(y)$ for the luminescence intensity at 571 nm in CMYLP:Dy (x = 0.10 and y = 0.05) under excitation at 385 nm, the relation between the luminescence intensity, I, and the substituted molar fraction, y, of Dy^{3+} at a sufficient dopant level, according to Dexter's law for evaluating multipolar energy transfer,[38] is given by

$$\log\left(\frac{I}{y}\right) = c - \left(\frac{\theta}{3}\right)\log(y)$$

where c is a constant, and θ = 6, 8, and 10 correspond to electric dipole–dipole (d–d), electric dipole–electric quadrupole (d–q), and electric quadrupole–electric quadrupole (q–q) interactions, respectively.[39] The θ value was calculated as 6.17, which is close to 6, indicating that the concentration quenching in this material was due to the d–d interaction.

Figure 5, panels a and b show the x and y dependence of emission spectra around the $^4F_{9/2} \rightarrow {}^6H_{15/2}$ and $^4F_{9/2} \rightarrow {}^6H_{13/2}$ transitions of Dy^{3+} ions in CMYLP:Dy. The emission intensity ratio ($I_{480\ nm}/I_{571\ nm}$) of these two transitions varied slightly with x (Figure 5c), while their peak shapes were almost the same. The substitution of Mg^{2+} to Ca^{2+} changed the spectral shape, produced an additional small peak at 496 nm, and increased the $I_{480\ nm}/I_{571\ nm}$ ratio by about 18%. It is likely that the increase of the $I_{480\ nm}/I_{571\ nm}$ ratio indicates that the large Ca^{2+} ions relaxed the structural distortion. These variations by

DOI: 10.1021/acsami.5b06208
ACS Appl. Mater. Interfaces 2015, 7, 21398–21407

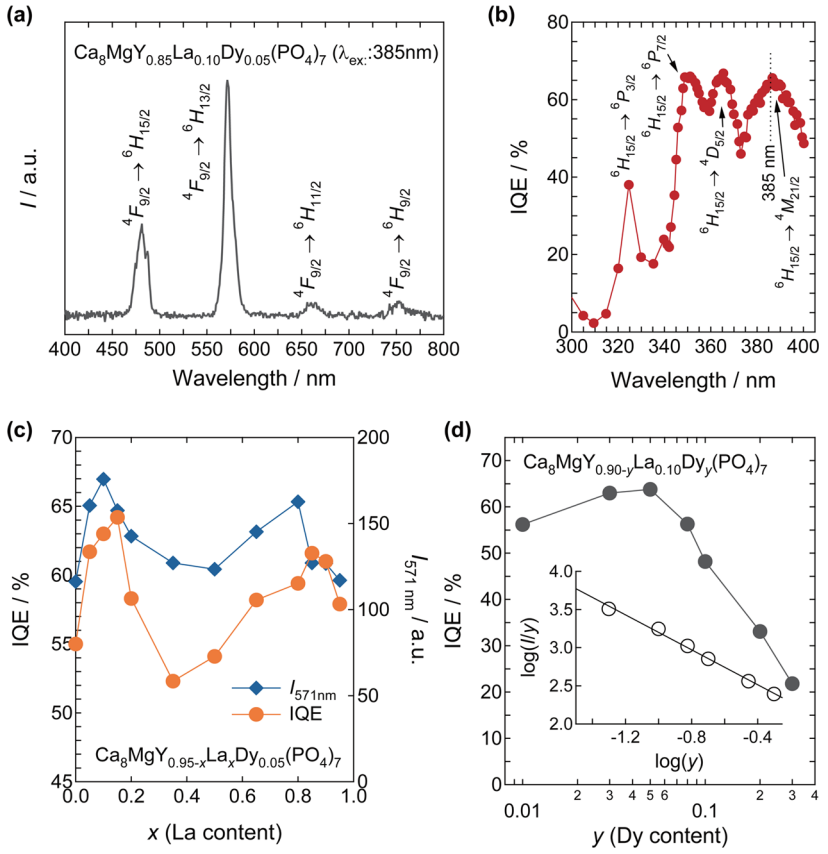

Figure 4. (a) Photoluminescence spectrum of CMYLP:Dy (x = 0.10 and y = 0.05) excited at 385 nm. (b) IQE of CMYLP:Dy (x = 0.10 and y = 0.05) as a function of wavelength. (c) IQE and integrated luminescence intensity at 571 nm for CMYLP:Dy (y = 0.05) as a function of concentration, x, under 385 nm excitation. (d) IQE for CMYLP:Dy (x = 0.10) as a function of concentration, y, under 385 nm excitation. The inset plot of $\log(I/y)$ versus $\log(y)$ shows the luminescence intensity at 571 nm in CMYLP:Dy (x = 0.10) under excitation at 385 nm. The line represents the fitting curve.

substitution of Mg^{2+}/Ca^{2+} ions mean that modification of M5 site also affected the crystal-field environment around the Dy^{3+}, resulting in the variation of luminescence of whitlockite-like hosts. The shape of the emission spectra of CMYLP:Dy did not depend on y, but the variation of $I_{480\ nm}/I_{571\ nm}$ was larger than that from variation of x. This difference between the y dependence and the dependence on substitution of Ca^{2+} to Mg^{2+} would be caused by increasing structural distortion around the Dy^{3+} due to its ionic size being smaller than that of Ca^{2+}.

3.2. Optical Properties of Dy-WLED and Plant Cultivation Tests. The Dy-WLED containing the CMYLP:Dy (x = 0.10 and y = 0.05) phosphor showed intense white light mainly consisting of three sharp emissions (Figure 6a): blue emission, which was the excess light from the excitation UV LED, and green−blue and yellow−orange luminescences from the CMYLP:Dy phosphor corresponding to the $^4F_{9/2} \rightarrow {}^6H_{15/2}$ and $^4F_{9/2} \rightarrow {}^6H_{13/2}$ transitions of Dy^{3+} ions. The CIE color coordinates and CCT were CIE(0.350,0.378) and 4919 K, respectively (Table 3 and Figure 6a). We used three other commercial LEDs as references: WLED1 (NVSW119BT, Nichia), WLED2 (TL1F1-WW1, Toshiba), and RGBWLED (LRTB C9TP, Osram). These had different types of spectra (Table 3 and Figure 6b,c). The emission spectra (Figure 6a,b) show big differences between the Dy-WLED and conventional LEDs, which emitted white light with CCT = 4000−13000 K (Table 3). The commercial WLEDs (WLED1 and WLED2) emitted light over almost the entire wavelength range of visible light because of the wide luminescence band of the phosphors in addition to the blue light from the excitation LEDs. In the RGBLED, there were three strong emissions at 458, 532, and 643 nm. We compared the effects of these different emission spectra on two types of plant growth: (1) a *Chlorella* cultivation test corresponding to photosynthesis under continuous LED illumination and (2) observations of bloom impediment by night-time LED illumination under a short-day condition for the short-day plant *Cosmos*.

First, the *Chlorella* cultivation test using the Dy-WLED, WLED1, WLED2, and RGBLED was carried out (Figure S1). The LEDs illuminated 3 mL of *Chlorella* dispersion in cultivation cells for 14 days at equivalent illuminance of 200 lm m^{-2} that is comparable to typical outdoor light at ground level. We observed color changes of the *Chlorella* dispersion (Figure 7a). While the dispersion was light green for the sample illuminated by the Dy-WLED, the samples illuminated by the other reference LEDs were much greener. The dried residue for grown *Chlorella* was weighed, and the weight of the sample illuminated by the Dy-WLED was much less than those of the other reference LEDs. The measured weights were 330 μg (a 66-fold increase from the dark reference) for WLED1, 433 μg (a 87-fold increase from the dark reference) for WLED2, 523 μg (a 105-fold increase from the dark reference) for RGBLED, and 176 μg (a 35-fold increase from the dark reference) for Dy-WLED (Table 4). Thus, the measured weight after illumination by the Dy-WLED was only 53%, 40%, and 33% of the weights for WLED1, WLED2, and RGBLED illumination, respectively.

DOI: 10.1021/acsami.5b06208
ACS Appl. Mater. Interfaces 2015, 7, 21398−21407

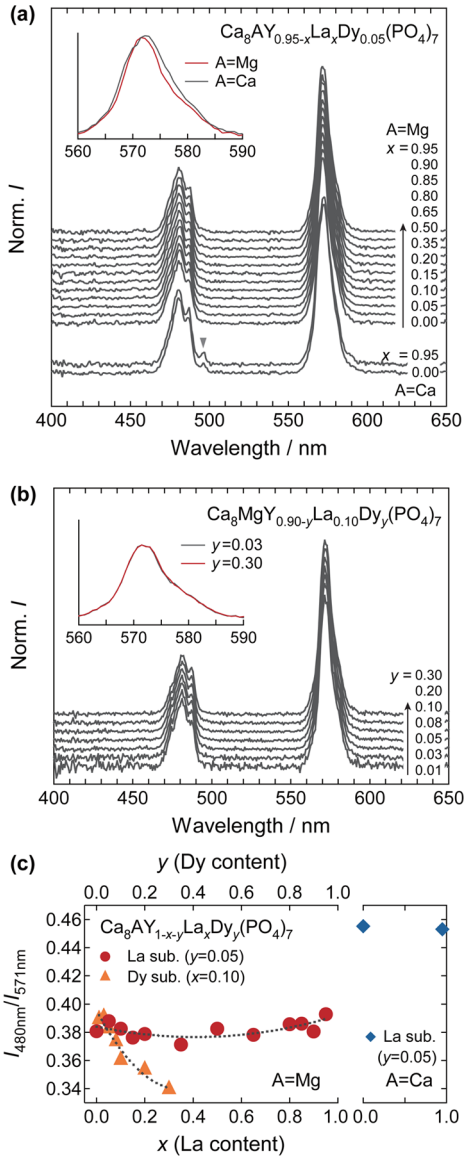

Figure 5. (a) x dependence of photoluminescence spectra of $Ca_8AY_{1-x}La_xDy_{0.05}(PO_4)_7$ (A = Mg and Ca) excited at 385 nm. (b) y dependence of photoluminescence spectra of $Ca_8MgY_{0.90-y}La_{0.10}Dy_y(PO_4)_7$ excited at 385 nm. (c) $I_{480\ nm}/I_{571\ nm}$ of $Ca_8AY_{1-x-y}La_xDy_y(PO_4)_7$ (A = Mg and Ca).

The data previously taken for same *Chlorella* cultivation conditions with illumination from WLED1, WLED2, WLED3, and Dy-WLED2, which used the $K_2Y_{0.97}Dy_{0.03}(WO_4)(PO_4)$ phosphor, are also plotted in Figure 7, panel a (the emission spectra of WLED3 and Dy-WLED2 are shown in Figures 6b and S3.).[15] The reductions of photosynthesis in *Chlorella* by the two Dy-based WLEDs are consistent.

The origin of reduced photosynthesis in the Dy-WLED has been reported as being due to the following reasons:[15] low correlation between the LED illumination and photosynthetic action spectra and especially a reduction in the Emerson effect,[40] which is a synergetic effect of illumination by multiwavelength bands, as a result of decreased red light illumination. Therefore, we introduce two indicators, C_{PS} and I_{red}:

$$C_{PS} = \int_{800nm}^{350nm} PS(x) \times I(x)\, dx$$

$$I_{red} = \int_{800nm}^{600nm} I(x)\, dx$$

where x is the wavelength, $PS(x)$ is a typical photosynthetic action spectrum (Figure S4),[41] and $I(x)$ is the LED emission spectra. The C_{PS} and I_{red} indicators were calculated by integrating to near-IR wavelengths from near-UV (350−800 nm) and from red (600−800 nm), respectively. These indicators for each LED are shown in Figure 7, panel b. The residue weight had a large correlation with I_{red}; therefore, our speculation that the reduction of I_{red} is dominant in the suppression of photosynthesis was strongly supported by these results. The Dy-WLED prepared in this study produced a 44% larger residue weight than the Dy-WLED2. Although the values of I_{red} for Dy-WLED and Dy-WLED2 were very similar, the value of C_{PS} for Dy-WLED was 19% higher than that for Dy-WLED2 due to a slightly larger amount of excess light from the excitation UV LED (Figure S3). Actually, light from the near UV to blue wavelength range also has a relatively large correlation to the photosynthetic action spectrum and fundamental chlorophyll *a* and *b* absorptions (Figure S4).[42] Therefore, dealing with excess excitation light would be very important in further reducing the photosynthesis effect.

We also carried out biocultivation experiments to study the inhibition of blooming impediment in short-day plants. Three *Cosmos* plants were cultivated for each of five conditions: a dark (nighttime) reference and illumination by WLED1, WLED2, RGBLED, and Dy-WLED LEDs. The LEDs were illuminated

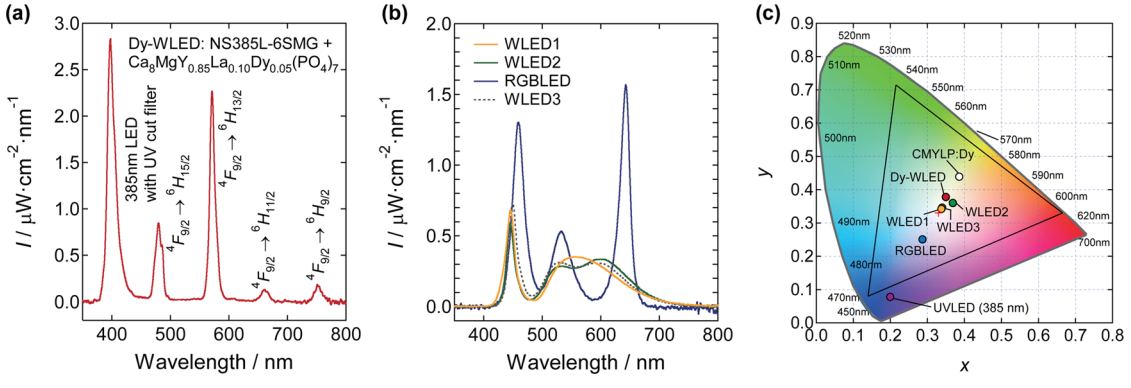

Figure 6. Emission spectral irradiance for (a) Dy-WLED using the CMYLP:Dy (x = 0.10 and y = 0.05) phosphor and (b) commercial LEDs (WLED1, WLED2, WLED3, and RGBLED). (c) CIE chromaticity diagram for the Dy-WLED, WLED1, WLED2, WLED3, RGBLED, and UVLED.

DOI: 10.1021/acsami.5b06208
ACS Appl. Mater. Interfaces 2015, 7, 21398−21407

Table 3. LEDs for Biocultivation Experiments

LED	manufacturer	model	CIE(x,y)	CCT
WLED1	Nichia	NVSW119BT	0.338,0.342	5204 K
WLED2	Toshiba	TL1F1-WH1	0.369,0.360	4199 K
WLED3 [15]	Toshiba	TL1F1-NW1	0.340,0.346	5266 K
RGBLED	Osram	LRTB C9TP	0.287,0.251	12560 K
UVLED	Nitride Semiconductors	NS385L-6SMG	0.200,0.078	
Dy-WLED		this work	0.357,0.374	4919 K

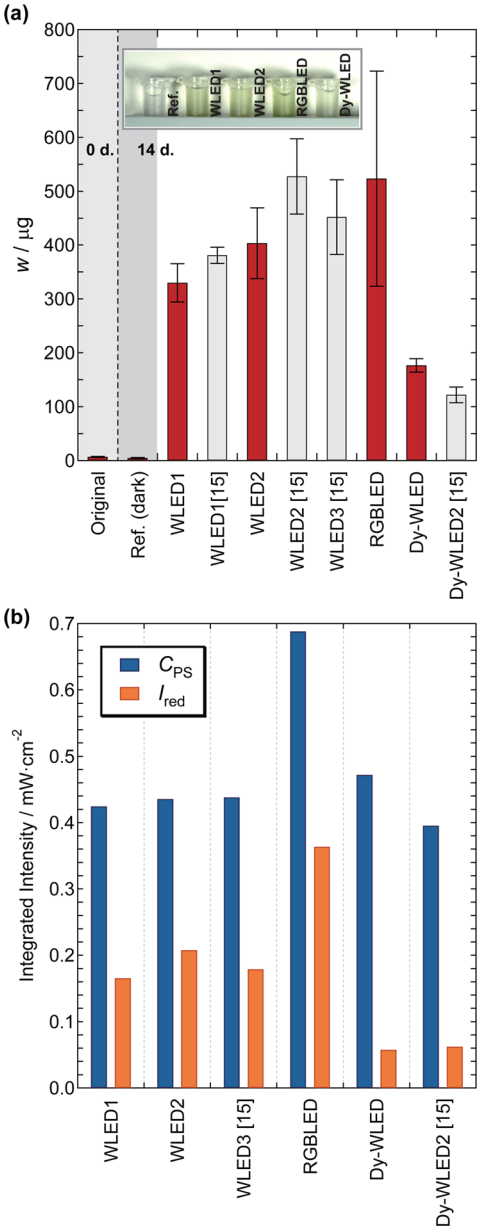

Figure 7. (a) Dried residue weight of the original sample of *Chlorella* (0 days), reference sample kept in the dark (14 days), and samples illuminated by WLED1, WLED2, RGBLED, and Dy-WLED at 200 lm m^{-2}. Data previously taken using WLED1, WLED2, WLED3, and Dy-WLED2, which used the $K_2Y_{0.97}Dy_{0.03}(WO_4)$ (PO_4) phosphor, and the same *Chlorella* cultivation conditions are also plotted.[15] The inset shows photographs of the *Chlorella* dispersions after 14 days at 200 lm m^{-2}. (b) C_{PS} and I_{red} for WLED1, WLED2, WLED3, RGBLED, Dy-WLED, and Dy-WLED2 at 200 lm m^{-2}.

Table 4. Residual Weight of Cultivated *Chlorella* under LED Illumination[a]

LED	w (μg)	w/w_{dark}	$w_{Dy\text{-}WLED}/w$
WLED1	330	66	0.53
WLED2	433	87	0.40
RGBLED	523	105	0.33
Dy-WLED	176	35	

[a]The w_{dark} and $w_{Dy\text{-}WLED}$ represent residual weights of dark reference and Dy-WLED illumination, respectively.

for 16 h at nighttime every day, and a fluorescent lamp was used as a proxy for sunlight illumination for 8 h during the day (Figure S5). The total numbers of blooms as a function of cultivation days were counted and are shown in Figures 8 and

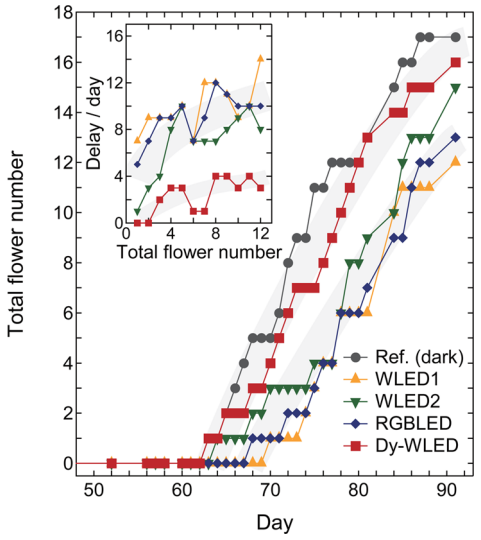

Figure 8. Total numbers of blooms of *Cosmos* as a function of cultivation days for dark reference, WLED1, WLED2, RGBLED, and Dy-WLED. The inset shows the delay in days as a function of total flower number.

S6. The dark reference plants showed the most rapid blooming pace from the 61st day. The Dy-WLED illuminated plants followed with 1−4 days delay, while further blooming delay was clearly observed for plants illuminated by the other LEDs (7−14 days delay). The origin of this inhibition of bloom impediment by the Dy-WLED can be explained as follows. The blooming of flowers strongly depends on one of the most important pigments of plants, phytochrome.[43] Phytochrome has two molecular forms, called Pr and Pfr. Both types of phytochrome have different absorption spectra, as shown in Figure 9, panel a. Pr is converted to Pfr by red light illumination at around 660 nm, and then it returns to being Pr for near-IR light at around 730 nm or darkness. This is a reversible reaction. There are absorption bands in Pr and Pfr in the near

DOI: 10.1021/acsami.5b06208
ACS Appl. Mater. Interfaces 2015, 7, 21398−21407

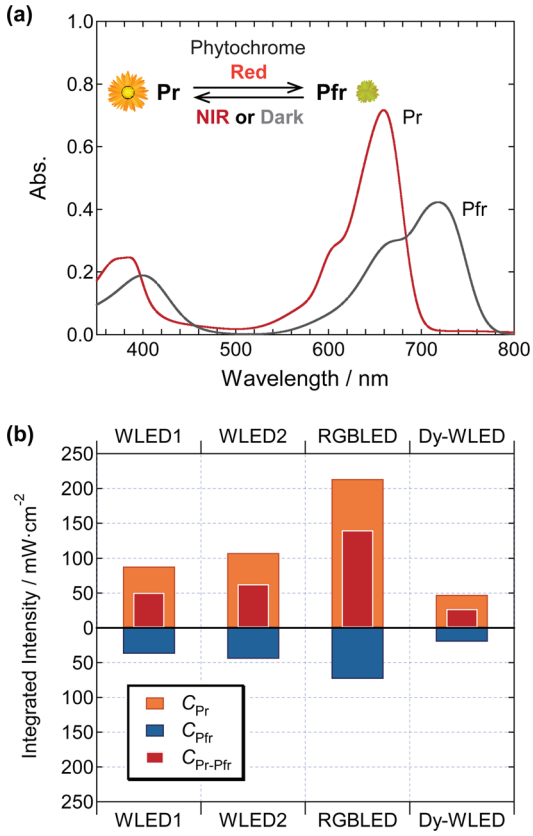

Figure 9. (a) Absorbance spectra of Pr and Pfr types of phytochrome molecules.[43] Adapted with permission from Elsevier. (b) Calculated C_{Pr}, C_{Pfr}, and C_{Pr-Pfr} values for WLED1, WLED2, RGBLED, and Dy-WLED.

UV range; however, these bands do not play a role in the Pr−Pfr reversible reaction. Short-day plants flower when a higher concentration of Pr compared to Pfr is accompanied by decreasing daytime length. Therefore, a relation between the nighttime illumination spectra and Pr/Pfr absorption has a very significant effect on blooming in short-day plants. We evaluated the relation using the following indicators:

$$C_{Pr(Pfr)} = \int_{800nm}^{500nm} Abs_{Pr(Pfr)}(x) \times I(x),$$

$$C_{Pr-Pfr} = C_{Pr} - C_{Pfr}$$

where x is the wavelength, $Abs_{Pr(Pfr)}(x)$ is the absorbance spectrum for Pr or Pfr molecules (Figure 9a),[43] and $I(x)$ is the LED emission spectra. The indicators C_{Pr} and C_{Pfr} were obtained by integration over green to near-IR wavelengths (500−800 nm) corresponding to the main absorbance bands of Pr and Pfr. The indicator C_{Pr-Pfr}, which is the difference between C_{Pr} and C_{Pfr}, roughly indicates the Pr concentration after the overall Pr−Pfr reaction. The calculated values of C_{Pr}, C_{Pfr}, and C_{Pr-Pfr} are shown in Figure 9, panel b. Both C_{Pr} and C_{Pr-Pfr} for the Dy-WLED were much less than those of the reference LEDs. The value of C_{Pr-Pfr} for the Dy-WLED was only 52%, 41%, and 19% of those for WLED1, WLED2, and RGBLED, respectively. The inhibition of bloom impediment observed for the Dy-WLED has a certain level of consistency with the C_{Pr-Pfr} values, suggesting that reducing red−near-IR illumination was effective for the inhibition of bloom impediment as well as for the suppression of photosynthesis. Thus, we have demonstrated two important functions of Dy-WLEDs by using the CMYLP:Dy phosphors: the reduction of photosynthesis and newly discovered inhibition of bloom impediment in short-day plants. Since the variation of Pr/Pfr concentration plays a fundamental role for bolting in long-day plants as well as for bloom impediment in short-day plants, Dy-WLEDs could suppress bolting in long-day plants as well.

Nevertheless, natural plant growth mechanisms are very complex and are based on functions of many pigments, so plants have evolved to use as wide a range of sunlight wavelengths as possible. Therefore, it is extremely hard to completely eliminate functions for plant growth under artificial visible light illumination, whatever light sources we choose. However, we have shown that the selective wavelengths emitted from Dy^{3+} ions can substantially reduce the correlation between illumination and plant growth, and in the near future, Dy-WLEDs can be expected to work as well as PHC-WLEDs for environmental protection.

4. CONCLUSION

We have prepared a new whitlockite-like Dy-phosphor $Ca_8MgY_{1-x-y}La_xDy_y(PO_4)_7$ (CMYLP:Dy). The CMYLP:Dy exhibited a yellow−white luminescence consisting of sharp emission peaks at 480, 571, 661, and 751 nm that can be assigned, respectively, to the $^4F_{9/2} \rightarrow {}^6H_{15/2}$, $^4F_{9/2} \rightarrow {}^6H_{13/2}$, $^4F_{9/2} \rightarrow {}^6H_{11/2}$, and $^4F_{9/2} \rightarrow {}^6H_{9/2}$ transitions in Dy^{3+} ions. The maximum IQE was 65.6% under 387 nm excitation light for x = 0.10 and y = 0.05. The x dependence of the IQE showed two maxima at x = 0.10−0.15 and 0.80−0.85, which could be due to the partial allowance of f−f forbidden transitions as a result of local lattice distortion around the Dy^{3+} ions originating from the La incorporation at near end members of CMYLP:Dy. Concentration quenching occurred for x > 0.05. The R_C value was 13.46 Å, and the d−d interaction was the dominant mechanism for concentration quenching. A WLED was fabricated from a UV LED emitting at 385 nm and the CMYLP:Dy phosphor; the CIE color coordinates and CCT were CIE(0.350,0.378) and 4919 K, respectively. Plant cultivation experiments on *Chlorella* photosynthetic growth and blooming tests of the short-day plant *Cosmos* were carried out using the prepared Dy-WLED and reference commercial LEDs. We found that the Dy-WLED reduced photosynthesis in *Chlorella* substantially and inhibited the bloom impediment of *Cosmos*. These effects especially originated from the reduction of red−near-IR emissions. Thus, we conclude that the Dy-WLED is a very promising candidate PHC-WLED that can be used for outdoor lights, which will lead to the protection of natural plant habitats.

■ ASSOCIATED CONTENT

Supporting Information

The Supporting Information is available free of charge on the ACS Publications website at DOI: 10.1021/acsami.5b06208.

Structural refinement data; XRD, emission, and absorbance spectra (PDF)

■ AUTHOR INFORMATION

Corresponding Author

*E-mail: t-nakajima@aist.go.jp.

Notes

The authors declare no competing financial interest.

DOI: 10.1021/acsami.5b06208
ACS Appl. Mater. Interfaces 2015, 7, 21398−21407

REFERENCES

(1) Akasaki, I.; Amano, H. Breakthroughs in Improving Crystal Quality of GaN and Invention of the p-n Junction Blue-Light-Emitting Diode. *Jpn. J. Appl. Phys.* **2006**, *45*, 9001−9010.

(2) Schlotter, P.; Schmidt, R.; Schneider, J. Luminescence Conversion of Blue Light Emitting Diodes. *Appl. Phys. A: Mater. Sci. Process.* **1997**, *64*, 417−418.

(3) Smet, P. F.; Parmentier, A. B.; Poelman, D. Selecting Conversion Phosphors for White Light-Emitting Diodes. *J. Electrochem. Soc.* **2011**, *158*, R37−R54.

(4) Lu, C.-H.; Jagannathan, R. Cerium-Ion-Doped Yttrium Aluminum Garnet Nanophosphors Prepared Through Sol-Gel Pyrolysis for Luminescent Lighting. *Appl. Phys. Lett.* **2002**, *80*, 3608−3610.

(5) Xie, R.-J.; Hirosaki, N.; Kimura, N.; Sakuma, K.; Mitomo, M. 2-Phosphor-Converted White Light-Emitting Diodes Using Oxynitride/Nitride Phosphors. *Appl. Phys. Lett.* **2007**, *90*, 191101−1−191101−3.

(6) Pust, P.; Weiler, V.; Hecht, C.; Tücks, A.; Wochnik, A. S.; Henß, A.-K.; Wiechert, D.; Scheu, C.; Schmidt, P. J.; Schnick, W. Narrow-Band Red-Emitting $Sr[LiAl_3N_4]:Eu^{2+}$ as A Next-Generation LED-Phosphor Material. *Nat. Mater.* **2014**, *13*, 891−896.

(7) Ye, S.; Xiao, F.; Pan, Y. X.; Ma, Y. Y.; Zhang, Q. Y. Phosphors in Phosphor-Converted White Light-Emitting Diodes: Recent Advances in Materials, Techniques and Properties. *Mater. Sci. Eng., R* **2010**, *71*, 1−34.

(8) Xie, R.-J.; Hirosaki, N. Silicon-Based Oxynitride and Nitride Phosphors for White LEDs−A Review. *Sci. Technol. Adv. Mater.* **2007**, *8*, 588−600.

(9) Nakajima, T.; Isobe, M.; Tsuchiya, T.; Ueda, Y.; Kumagai, T. Direct Fabrication of Metavanadate Phosphor Films on Organic Substrates for White-Light-Emitting Devices. *Nat. Mater.* **2008**, *7*, 735−740.

(10) Nakajima, T.; Shinoda, K.; Tsuchiya, T. Single-LED Solar Simulator for Amorphous Si and Dye-Sensitized Solar Cells. *RSC Adv.* **2014**, *4*, 19165−19171.

(11) Nagayama Electric Industrial Co., LTD. JP Patent JP4670108, 2011.

(12) Tokimasa, F.; Suedomi, M. Effect of the Night-Illumination by Electric Lamps on the Growth and the Yields of Paddy Rice. *Nippon Sakumotsu Gakkai Kiji* **1971**, *40*, 241−246.

(13) Ishikawa, R.; Tamaki, S.; Yokoi, S.; Inagaki, N.; Shinomura, T.; Takano, M.; Shimamoto, K. Suppression of the Floral Activator Hd3a Is the Principle Cause of the Night Break Effectin Rice. *Plant Cell* **2005**, *17*, 3326−3336.

(14) Yamaguchi University. WO Patent WO2011/052462, 2011.

(15) Nakajima, T.; Hanawa, H.; Tsuchiya, T. Plant Habitat-Conscious White Light-Emitting Devices: Dy^{3+}-Emission Considerably Reduces Involvement in Photosynthesis. *J. Mater. Chem. C* **2015**, *3*, 3371−3378.

(16) Marciniak, L.; Hreniak, D.; Strek, W. Controlling Luminescence Colour Through Concentration of Dy^{3+} Ions in $LiLa_{1-x}Dy_xP_4O_{12}$ Nanocrystals. *J. Mater. Chem. C* **2014**, *2*, 5704−5708.

(17) Zhang, X.; Lu, Z.; Meng, F.; Hu, L.; Xu, X.; Lin, J.; Tang, C. Luminescence Properties of $Ca_3Si_2O_7:Dy^{3+}$ Phosphor for White Light-Emitting Diodes. *Mater. Lett.* **2012**, *79*, 292−295.

(18) Yang, M.; Zhao, X.; Ji, Y.; Liu, F.; Liu, W.; Sun, J.; Liu, X. Hydrothermal Approach and Luminescent Properties for the Synthesis of Orthoniobates $GdNbO_4:Ln^{3+}$ (Ln = Dy, Eu) Single Crystals under High-Temperature Conditions. *New J. Chem.* **2014**, *38*, 4249−4257.

(19) Kaczmarek, A. M.; Van Hecke, K.; Van Deun, R. Enhanced Luminescence in Ln^{3+}-doped Y_2WO_6: (Sm, Eu, Dy) 3D Microstructures Through Gd^{3+} Codoping. *Inorg. Chem.* **2014**, *53*, 9498−9508.

(20) Zhou, Y.; Yan, B.; He, X.-H. Controlled Synthesis and Up/Down-Conversion Luminescence of Self-Assembled Hierarchical Architectures of Monoclinic $AgRE(WO_4)_2:Ln^{3+}$ (RE = Y, La, Gd, Lu; Ln = Eu, Tb, Sm, Dy, Yb/Er, Yb/Tm). *J. Mater. Chem. C* **2014**, *2*, 848−855.

(21) Shang, M.; Li, G.; Kang, X.; Yang, D.; Lin, J. Synthesis and Luminescent Properties of $Li_3Ba_2Y_3(MoO_4)_8:Ln^{3+}$ (Ln = Eu, Tb, Dy) Phosphors for UV-LEDs. *J. Electrochem. Soc.* **2011**, *158*, H565−H571.

(22) Izumi, F.; Momma, K. Three-Dimensional Visualization in Powder Diffraction. *Solid State Phenom.* **2007**, *130*, 15−20.

(23) Momma, K.; Izumi, F. VESTA 3 for three-dimensional visualization of crystal volumetric and morphology data. *J. Appl. Crystallogr.* **2011**, *44*, 1272−1276.

(24) Adcock, C. T.; Hausrath, E. M.; Forster, P. M.; Tschauner, O.; Sefein, K. J. Synthesis and Characterization of the Mars-Relevant Phosphate Minerals Fe- and Mg-Whitlockite and Merrillite and a Possible Mechanism that Maintains Charge Balance during Whitlockite to Merrillite Transformation. *Am. Mineral.* **2014**, *99*, 1221−1232.

(25) Benhamou, R. A.; Bessiere, A.; Wallez, G.; Viana, B.; Elaatmani, M.; Daoud, M.; Zegzouti, A. New Insight in the Structure-Luminescence Relationships of $Ca_9Eu(PO_4)_7$. *J. Solid State Chem.* **2009**, *182*, 2319−2325.

(26) Lazoryak, B. I.; Strunenkova, T. V.; Golubev, V. N.; Vovk, E. A.; Ivanov, L. N. Triple Phosphates of Calcium, Sodium and Trivalent Elements with Whitlockite-Like Structure. *Mater. Res. Bull.* **1996**, *31*, 207−216.

(27) Bessière, A.; Benhamou, R. A.; Wallez, G.; Lecointre, A.; Viana, B. Site Occupancy and Mechanisms of Thermally Stimulated Luminescence in $Ca_9Ln(PO_4)_7$ (*Ln* = Lanthanide). *Acta Mater.* **2012**, *60*, 6641−6649.

(28) Wu, X.; Liang, Y.; Chen, R.; Liu, M.; Cheng, Z. Photoluminescence Properties of Emission-Tunable $Ca_9Y(PO_4)_7$: Tm^{3+}, Dy^{3+} Phosphor for White Light Emitting Diodes. *Mater. Chem. Phys.* **2011**, *129*, 1058−1062.

(29) Shannon, R. D.; Prewitt, C. T. Effective Ionic Radii in Oxides and Fluorides. *Acta Crystallogr., Sect. B: Struct. Crystallogr. Cryst. Chem.* **1969**, *25*, 925−946.

(30) Gu, F.; Wang, S. F.; Lü, M. K.; Zhou, G. J.; Xu, D.; Yuan, D. R. Structure Evaluation and Highly Enhanced Luminescence of Dy^{3+}-Doped ZnO Nanocrystals by Li^+ Doping Via Combustion Method. *Langmuir* **2004**, *20*, 3528−3531.

(31) Krishna, K. M.; Anoop, G.; Jayaraj, M. K. Host Sensitized White Luminescence from $ZnGa_2O_4:Dy^{3+}$ Phosphor. *J. Electrochem. Soc.* **2007**, *154*, J310−J313.

(32) Kyômen, T.; Sakamoto, R.; Sakamoto, N.; Kunugi, S.; Itoh, M. Photoluminescence Properties of Pr-Doped $(Ca,Sr,Ba)TiO_3$. *Chem. Mater.* **2005**, *17*, 3200−3204.

(33) Nakajima, T.; Yoshizawa, H.; Ueda, Y. *A*-site Randomness Effect on Structural and Physical Properties of Ba-Based Perovskite Manganites. *J. Phys. Soc. Jpn.* **2004**, *73*, 2283−2291.

(34) Nakajima, T.; Ueda, Y. 1000% Colossal Magnetoresistance at Room Temperature in the A-site Ordered Perovskite Manganites, $Sm_{1-x}La_{x+y}Ba_{1-y}Mn_2O_6$. *J. Appl. Phys.* **2005**, *98*, 046108−1−046108−3.

(35) Blasse, G. Energy Transfer in Oxidic Phosphors. *Phys. Lett. A* **1968**, *28*, 444−445.

(36) Antipeuko, B. M.; Bataev, I. M.; Ermolaev, V. L.; Lyubimov, E. I.; Privalova, T. A. Ion-to-Ion Radiationless Transfer of Electron Excitation Energy Between Rare-Earth Ions in $POCl_3$-$SnCl_4$. *Opt. Spektrosk.* **1970**, *29*, 177−180.

(37) Blasse, G.; Grabmaier, B. *Luminescent Materials*; Springer Verlag: Berlin, Heidelberg, 1994.

(38) Dexter, D. L. Theory of Sensitized Luminescence in Solids. *J. Chem. Phys.* **1953**, *21*, 836−1−836−15.

(39) Van Uitert, L. G.; Dearborn, E. F.; Rubin, J. J. Mechanisms of Energy Transfer Involving Trivalent Tb and Nd in Sodium Rare-Earth Tungstates. *J. Chem. Phys.* **1967**, *47*, 547−553.

(40) Emerson, R.; Lewis, C. M. The Dependence of the Quantum Yield of Chlorella Photosynthesis on Wave Length of Light. *Am. J. Bot.* **1943**, *30*, 165−178.

(41) Inada, K. Action Spectra for Photosynthesis in Higher-Plants. *Plant Cell Physiol.* **1976**, *17*, 355−365.

(42) Ikegam, I.; Kamiya, A. Presence of the Photoactive Reaction-Center Chlorophyll of PSI (P700) in Dark-Grown Cells of a

DOI: 10.1021/acsami.5b06208
ACS Appl. Mater. Interfaces 2015, 7, 21398−21407

Chlorophyll-Deficient Mutant of Chlorella Kessleri. *Plant Cell Physiol.* **1998**, *39*, 1087−1092.
(43) Anderson, G. R.; Jenner, E. L.; Mumford, F. E. Optical Rotatory Dispersion and Circular Dichroism Spectra of Phytochrome. *Biochim. Biophys. Acta, Protein Struct.* **1970**, *221*, 69−73.

DOI: 10.1021/acsami.5b06208
ACS Appl. Mater. Interfaces 2015, 7, 21398−21407